Published in final edited form as:
Langmuir. 2012 June 5; 28(22): 8456–8462. doi:10.1021/la301241s.

Inter-kingdom Signaling: Integration, Conformation and Orientation of *N*-Acyl-L-Homoserine Lactones in Supported Lipid Bilayers

Christoph Barth[1], **Dorota Jakubczyk**[2], **Adam Kubas**[3], **Frances Anastassacos**[1], **Gerald Brenner-Weiss**[2], **Karin Fink**[3], **Ute Schepers**[1], **Stefan Bräse**[4], and **Patrick Koelsch**[5,*]

[1]Institute for Toxicology and Genetics, Karlsruhe Institute of Technology, Postfach 3640, 76021 Karlsruhe, Germany

[2]Institute for Functional Interfaces, Karlsruhe Institute of Technology, Postfach 3640, 76021 Karlsruhe, Germany

[3]Institute of Nanotechnology, Karlsruhe Institute of Technology, Postfach 3640, 76021 Karlsruhe, Germany

[4]Institute of Organic Chemistry, Karlsruhe Institute of Technology, Postfach 3640, 76021 Karlsruhe, Germany

[5]National ESCA and Surface Analysis Center for Biomedical Problems, Department of Bioengineering, University of Washington, Box 35170, Seattle, WA 98195-1750

Abstract

N-Acyl-L-homoserine lactones (AHLs) are small cell-to-cell signaling molecules involved in the regulation of population density and local gene expression in microbial communities. Recent evidence shows that contact of this signaling system, usually referred to as quorum sensing, to living eukaryotes results in interactions of AHL with host cells in a process termed "inter-kingdom signaling". So far details of this process and the binding site of the AHLs remain unknown; both an intracellular and a membrane-bound receptor seem possible, the first of which requires passage through the cell membrane. Here, we used sum-frequency-generation (SFG) spectroscopy to investigate the integration, conformation, orientation, and translocation of deuterated *N*-Acyl-L-homoserine lactones (AHL-d_n) with varying chain length (8, 12, and 14 C atoms) in lipid bilayers consisting of a 1:1 mixture of POPC:POPG supported on SiO_2 substrates (prepared by vesicle fusion). We found that all AHL-d_n derivatives are well-ordered within the supported lipid bilayer (SLB) in a preferentially all-trans conformation of the deuterated alkyl chain and integrated into the upper leaflet of the SLB with the methyl terminal groups pointing downwards. For the bilayer system described above, no flip-flop of AHL-d_n from the upper leaflet to the lower one could be observed. Spectral assignments and interpretations were further supported by Fourier transform infrared and Raman spectroscopy.

Keywords

Inter-kingdom signaling, *N*-Acyl-L-homoserine lactones (AHLs); sum-frequency-generation (SFG) spectroscopy; supported lipid bilayers (SLBs); infrared and Raman spectroscopy

*Corresponding author. koelsch@uw.edu.

INTRODUCTION

Bacteria are omnipresent in daily life often forming microcolonies within a polysaccharide matrix attached to a surface.[1–3] These biofilms are ubiquitous and can be found in all non-sterile aqueous environments or habitats, including natural and technical surfaces such as pipelines, membranes, filters, teeth, and medical implant surfaces. From a medical perspective, biofilms are a common cause of persistent and serious bacterial infections with profound implications for the patient.[4–6] Biofilm formation is a well-controlled process involving signaling molecules produced and secreted by bacteria in a regulating system termed quorum sensing (QS).[7–9]

The behavior of *N*-Acyl-L-homoserine lactones (AHLs) as QS molecules in the biofilm formation of *Pseudomonas aeruginosa* is particularly well studied.[10] Besides AHL involvement in QS, it was found that AHLs also allow communication between bacteria and eukaryotic hosts in a process termed "inter-kingdom signaling".[7, 11, 12] For example, *N*-(3-oxododecanoyl)-L-homoserine lactone, a prominent QS member of the AHL class, exhibits several immune modulatory effects, *e.g.* the ability to down-regulate defense-relevant functions of the immune system,[13–15] but also the promotion of the host´s defense by inducing chemotaxis of human polymorphonuclear neutrophils (PMNs) *in vitro*.[16] These observations indicate that both extracellular membrane-associated and intracellular receptors are involved. Moreover, the method by which AHLs enter mammalian cells is unexplained. Here, both a receptor-mediated path and a non-receptor mediated process seem feasible.[17, 18] However, an interaction with intracellular components would require AHL molecules to bypass the cell membrane, a process involving the integration of AHL into the lipid bilayer.

Recently, we reported on the preparation of deuterated *N*-(3-oxododecanoyl-d_{17})-L-homoserine lactone and its integration into supported lipid bilayers (SLBs) studied by vibrational sum-frequency-generation (SFG) spectroscopy.[19] This technique precludes signals resulting from arrangements, which are either isotropic or possess a center of inversion.[20, 21] In a symmetric SLB, the sum of IR transition dipole moments corresponding to methyl and methylene vibrations vanishes, whereas the integration of molecules into the bilayer in an asymmetric fashion potentially leads to an SFG signal.[22–45]

Here, we investigate the integration, conformation, orientation, and flip-flop behavior of three deuterium labeled AHL derivatives (Fig. 1) exposed to SLBs (1:1 mixture of POPC:POPG) prepared by vesicle fusion on SiO_2 coated substrates. Spectral assignments and interpretations of SFG signals were further supported by solid state Fourier transform infrared (FTIR) and Raman measurements.

EXPERIMENTAL SECTION

Preparation of AHL-d_n and supported lipid bilayers

AHL-d_n and their analytical evaluation were described in detail in our recent publication.[19] The method used is based on that described by Chhabra et al.[13] A two-step procedure towards deuterated *N*-acyl-l-homoserine lactones with varying chain lengths, starting from commercially available deuterated fatty acids, was described. This included the acylation of Meldrum's acid, followed by amidation.

Model lipid membranes were prepared by vesicle fusion from a 1-palmitoyl-2-oleoyl-*sn*-glycero-3-phosphocholine:1-palmitoyl-2-oleoyl-*sn*-glycero-3-phospho-(1'-*rac*-glycerol) 1:1 mixture (Avanti Polar Lipids, Alabaster, USA). Briefly, appropriate amounts of lipids solved in chloroform were mixed in a glass vial to obtain a final lipid mass of 2.5 mg. Chloroform

was evaporated by a gentle stream of nitrogen whilst constantly rotating the vial to obtain a thin uniform lipid film. The glass vial was then placed in a desiccator under constant vacuum drain for at least 2 hrs. The lipid film was rehydrated in 100mM NaCl, 10 mM Tris*HCl (pH 8) with enough buffer to obtain a lipid concentration of 2.5 mg/mL. The pH was adjusted to 8 with hydrochloric acid (HCl).[46] Small unilamellar vesicles (SUV) were obtained by extruding the lipid emulsion through polycarbonate membranes with 100 nm pore size at least 11 times using a commercially available extruder (Miniextruder, Avanti Polar Lipids Inc.).[47]

All lipid bilayers were formed on the same quartz crystal microbalance sensor (Q-Sense AB, Gothenburg, Sweden) with a 50 nm silicon dioxide layer and a 200 nm gold sublayer. Prior to usage, substrates were cleaned by immersion in 10 mM sodium dodecyl sulfate (SDS) for 10 min, rinsing with copious amounts of DI water and ethanol and UV/ozone treatment for 30 min to render the SiO_2-layer hydrophilic. After ozone treatment, the substrates were directly transferred to a small petri dish containing enough Ca^{2+}/Tris buffer (100 mM NaCl, 10 mM Tris, and 10 mM $CaCl_2$) to cover the substrate. The SUV suspension was diluted to 0.1 mg/mL using a Ca/Tris buffer to promote the bilayer formation[48] and was injected over the Q-Sense sensor. After allowing for bilayer formation for 25 min, excess liposomes were removed by rinsing five times with phosphate buffered saline (PBS). AHL-d_n solved in a acetonitrile:water (1:1) solution was added and integrated for 10 min. The substrate was then washed with PBS according to the previously described procedure to remove excess AHL-d_n. SFG experiments were started immediately after washing by mounting the substrate in the Thin Layer Analysis cell.

SFG spectroscopy

Details on the SFG spectrometer and the thin-layer analysis (TLA) cell used in the experiments can be found elsewhere.[49–55] Briefly, a broadband IR pulse of 100 fs pulse duration was centered around 2200 cm^{-1} and spatially overlapped on the sample with an etalon shaped narrowband ps pulse at 800 nm to generate a potential SFG signal analyzed using a spectrograph with an attached CCD camera. Incident angles (relative to the surface normal) for the IR and 800 nm beams were adjusted to 55° and 60°, respectively. The fully temperature controlled TLA cell consists of a less than one μm thin water slab sandwiched in between the sample and a hemispherical prism (CaF_2) used to guide the laser beams.[50] The resulting SFG intensity reads

$$I_{SF} \propto \left|\chi^{(2)}\right|^2 I_{IR} I_{VIS} \tag{1}$$

with

$$\chi^{(2)} = \chi^{(2)}_{NR} + \chi^{(2)}_{R} = \chi^{(2)}_{NR} + \sum_k \left| \frac{A_k}{(\omega_{IR} - \omega_k) + i\Gamma_k} \right| e^{i\phi_k}, \tag{2}$$

where $\chi^{(2)}_{NR}$ is the second-order susceptibility of the metallic substrate, A_k the amplitude of the k-th resonance, ω_k its frequency and ϕ_k the phase difference between substrate and resonant response. Γ_k represents the line width of the vibration and I_{IR}, I_{VIS} the intensities of the two incident beams.

Due to Au presence in the substrate, the SFG spectrum contains non-resonant contributions from electronic transitions. These can be suppressed by temporally separating the IR and Raman processes involved in the generation of SF signals. The 100 fs and about 30 μm long IR pulse is populating vibrational states, which are up-converted by a 300 fs delayed time asymmetric and narrowband visible beam to generate the SF response. In this temporal

order, IR and Vis beams are not simultaneously present at the surface to generate electronic transitions at the SF, effectively suppressing non-resonant signals from the metal substrate.[56–59] Background suppressed spectra were used to identify peak positions (ω_k), which were then given as parameters for the fit of the spectra with non-resonant background to determine the phases ϕ_k using Eq. (2). A potential phase shift induced by the 50 nm SiO_2 layer was neglected in our analysis.

Background-suppressed SFG spectra were recorded for 45 s and smoothed with a Savitzky–Golay routine using 15 data points. Non background-suppressed spectra were acquired with 90s accumulation time and used as is. All spectra were recorded in *p* polarizations for all beams (SFG, Vis, and IR) and normalized to their respective acquisition time. It should be noted that similar phases have been reported for *ssp* (*s* polarization for SFG and Vis beams) and *ppp* polarization spectra,[61] however, the latter combination probes more than one element of $\chi^{(2)}_{res}$ and relative phases may depend not only on the sign, but also the relative magnitude of the different tensor elements.

Peak positions were calibrated by comparison to an SFG spectrum obtained from a deuterated dodecanethiol self-assembled monolayer on Au. Time dependent studies were performed in background-suppressed mode and recorded every 15 min for 5h.

IR and Raman spectroscopy

IR and Raman spectra were recorded with the use of a Bruker Vertex 80 FTIR spectrometer (Bruker Optik GmbH, Ettlingen, Germany) with a single reflection "Golden Gate" diamond ATR sampling unit (Specac, UK). Additionally, Raman spectra were recorded with the use of a Bruker Senterra Raman microscope (Bruker Optics GmbH, Ettlingen, Germany), laser: excitation wavelength 785 nm, power 50 mw, 20× Objective (Olympus Mplan) = spot size 5 μm. IR spectra were recorded using a Bruker Hyperion 3000 FTIR Microscope, 15× reflection objective, spot size = 40μm.

RESULTS AND DISCUSSIONS

Integration of AHLs-d_n into the SLB

To investigate the integration of AHLs-d_n into the SLB, we examined SFG signals from a AHL-d_9 solution in contact with the SiO_2 substrate and (separately) AHL-d_n solutions with an SLB on SiO_2. Fig. 2 shows the SFG signal in the CD vibrational region for AHL-d_9 alone (flat line) and three derivatives of AHL-d_n in the presence of the SLB. Since isotropic, AHL-d_9 in solution does not generate a signal. No signal is generated for solvent and SLB alone either.[19] In contrast, the three AHL-d_n derivatives give rise to distinct bands in the presence of the lipid bilayer showing all compounds to integrate in the membrane. Unlike most linear optical techniques, order and number density are interlinked in SFG signals and further techniques are required to quantify the amount of AHL-d_n in the SLB. At this stage, we note that the SFG intensity increases with an increasing number of carbon atoms in the aliphatic chain indicating a higher amount and/or greater order of AHL-d_n in the SLB for longer chain lengths. The prominent peaks are located around 2140, 2190, and 2220 cm^{-1} for AHL-d_{21} and AHL-d_{17}, with the lower frequency band shifted to 2125 cm^{-1} for the AHL-d_9 derivative.

Conformation of AHL-d_n within the SLB

An SFG signal is only generated for bands that are both IR and Raman active. Fig. 3 shows a comparison between SFG spectra from incorporated AHL-d_n and IR and Raman spectra obtained from AHL-d_n in the solid state. Due to the higher number of methylene over methyl groups in AHL-d_{21}, the IR spectrum is dominated by CD_2 vibrations located at 2200

(antisymmetric, d^-) and 2100 cm^{-1} (symmetric, d^+). The spectral contributions that become more prominent with shorter chain lengths can be associated to CD_3 vibrations and are marked as vertical lines in Fig. 3. The position for these peaks are around 2125, 2140, 2190, and 2220 cm^{-1} and coincide perfectly to the ones detected in the SFG spectra of incorporated AHL-d_n shown in Fig. 2. The selection rules for second-order nonlinear optical processes dictate that molecular arrangements possessing inversion symmetry cannot generate an SF signal. Note that an alkane chain in all-trans configuration is symmetric with a center in-between carbon atoms. The absence of CD_2 contributions in the SFG spectra is therefore a strong indication that the aliphatic chain in the AHL-d_n derivatives is in an all-trans configuration when integrated into the membrane. This is indicative of a highly ordered conformation of AHL-d_n in the bilayer without gauche defects and kinks that would otherwise lead to the presence of CD_2 bands.[27, 60]

Orientation of AHL-d_n within the SLB

The understanding of AHL-d_n-lipid bilayer interactions necessitates the determination of the leaflet in which AHL-d_n is located. A reliable indicator of the AHL-d_n location is the orientation of the terminal deuterated methyl group. A terminal group directed towards the substrate is indicative of AHL-d_n in the upper leaflet, whereas a terminal group oriented away from the underlying substrate indicates a position in the lower leaflet. The orientation of the terminal methyl groups is closely related to the phase ϕ_k of the corresponding vibrational mode; a destructive phase (*e.g.* a dip in the spectrum) results when the methyl group is pointing away from the substrate, whereas a constructive phase (*e.g.* a peak in the spectrum) is an indicator of orientation towards the surface.[27, 61] The phases were determined by fitting the non background-suppressed SFG spectra shown in Fig. 4 by using Eq.(2). The peak at 2220 cm^{-1} has been previously assigned to CD_3 antisymmetric vibrations (r^-)[27, 60, 62] and is in accordance to the IR and Raman spectra of the shorter chain length AHL-d_9 spectra (Fig. 3). The results of the r^- vibration of different AHL-d_n derivatives are shown in Tab. 1. The determined phase for all three derivatives is close to constructive interference values corresponding to a dipole moment pointing towards the surface. The associated vibration of the terminal methyl group must therefore be directed towards the gold substrate indicating that AHL-d_n is located primarily in the upper leaflet of the bilayer.

Considering that all AHL-d_n are similarly ordered within the bilayer - a reasonable assumption from the absence of CD_2 vibrations in the SFG spectrum and similar orientations of the terminal group - an increased intensity with chain length (see. Fig. 2) can be related to a higher amount of integrated AHL-d_n in the bilayer, rather than ordering effects. It follows that less AHL-d_9 molecules are integrated into the bilayer, most likely because of a favorable balance between hydrophobic and hydrophilic moieties to remain in the aqueous phase.

Flip-flop of AHL-d_n within the SLB

SFG spectra in background-suppressed mode were recorded for 5 hours for all three AHL-d_n derivatives in the presence of the SLB. The corresponding integrated SFG intensities were normalized with respect to their initial values and plotted against time (Fig. 5). The overall intensity of each AHL-d_n derivative tends to decrease only slightly over time. To further quantify the flip-flop of incorporated AHL-d_n, the obtained intensity is considered a measure of the population difference of upper to lower bilayer leaflet yielding

$$I_{SFG} \propto (N_U - N_L)^2, \quad (3)$$

with N_U and N_L denoting the numbers of AHL-d_n molecules in the upper and lower leaflet, respectively. The process of a potential AHL-d_n flip-flop was assumed to be unimolecular with an equal and time independent rate constant k.[26] When at the beginning of the experiment, $N_U = 1$ and $N_L = 0$, the first time derivative of the lower leaflet's population can be written as

$$\frac{dN_L}{dt} = kN_U - kN_L = -k(2N_L - 1) \quad (4)$$

Integrating Eq. (4) and introducing it into Eq. (3) yields the following proportionality

$$I \propto \exp(-4kt) \quad (5)$$

The integrated overall intensity as plotted in Fig. 6 was fitted with a function based on Eq. (5). The half-life of the AHL-d_n flip-flop process can then be determined according to

$$T_{1/2} = \frac{\ln 2}{2k} \quad (6)$$

The results of the fit and the respective half-lives are given in Tab. 2. From Fig. 5 and Tab. 2, it is clear that a significant flipping process does not occur within the time scale (5h) used in these experiments. All AHL-d_n derivatives remain in the upper leaflet with little or no spectral changes in the final signals (data not shown). This should be related to different diffusion constants in the lower leaflet as a result of its close proximity to the SiO_2 substrate. It is also possible that the mismatch in chain lengths for lipids and AHL-d_n leads to a barrier making flipping of AHL unlikely.

CONCLUSION

We studied the integration, conformation, orientation, and flipping behavior of the three AHL-d_n derivatives within lipid bilayers on the basis of model membranes with a POPC:POPG 1:1 mixture on a solid hydrophilic support using nonlinear optical SFG spectroscopy. All AHL-d_n derivatives integrate into the upper leaflet of the lipid bilayers in a well-ordered all-trans conformation with a mean orientation of the terminal CD_3 groups towards the surface (parallel to the surface normal). An increased amount of incorporated AHL-d_n was found for longer chain lengths, which may result from the decreased ratio of hydrophilic head to aliphatic tail making it more favorable for short-chain AHLs-d_9 to remain in solution. Flip-flop or translocation of AHL within the membrane was not observed for the conditions and lipid system used in these experiments. Further studies in this direction should include different lipid systems, temperatures, and/or potential receptor candidates for AHL.

Acknowledgments

Financial support from the Helmholtz Program BioInterfaces is gratefully acknowledged. We thank Stefan Heissler from Karlsruhe Institute of Technology (KIT), Institute of Functional Interfaces (IFG) for help with IR and Raman spectral acquisition. P.K. acknowledges support from NIH grant EB-002027 to the National ESCA and Surface Analysis Center for Biomedical Problems.

REFERENCES

1. Costerton JW, Stewart PS, Greenberg EP. Bacterial biofilms: A common cause of persistent infections. Science. 1999; 284(5418):1318–1322. [PubMed: 10334980]
2. Davey ME, O'Toole GA. Microbial biofilms: from ecology to molecular genetics. Microbiol. Mol. Biol. Rev. 2000; 64(4):847–867. [PubMed: 11104821]
3. Krumbein, WE.; Paterson, DM.; Zavarzin, GA. Fossil and recent biofilms : a natural history of life on Earth. Dordrecht; Boston: Kluwer Academic Publishers; 2003. p. xxip. 482
4. Costerton JW, Cheng KJ, Geesey GG, Ladd TI, Nickel JC, Dasgupta M, Marrie TJ. Bacterial biofilms in nature and disease. Annu. Rev. Microbiol. 1987; 41:435–464. [PubMed: 3318676]
5. Marrie TJ, Costerton JW. Morphology of bacterial attachment to cardiac pacemaker leads and power packs. J. Clin. Microbiol. 1984; 19(6):911–914. [PubMed: 6470101]
6. Tenney JH, Moody MR, Newman KA, Schimpff SC, Wade JC, Costerton JW, Reed WP. Adherent Microorganisms on Lumenal Surfaces of Long-term Intravenous Catheters: Importance of Staphylococcus epidermidis in Patients With Cancer. Arch. Intern. Med. 1986; 146(10):1949–1954. [PubMed: 3767541]
7. Cooley M, Chhabra SR, Williams P. N-Acylhomoserine lactone-mediated quorum sensing: a twist in the tail and a blow for host immunity. Chem. Biol. 2008; 15(11):1141–1147. [PubMed: 19022174]
8. Juhas M, Eberl L, Tummler B. Quorum sensing: the power of cooperation in the world of Pseudomonas. Environ. Microbiol. 2005; 7(4):459–471. [PubMed: 15816912]
9. Schuster M, Greenberg EP. A network of networks: quorum-sensing gene regulation in Pseudomonas aeruginosa. Int. J. Med. Microbiol. 2006; 296(2–3):73–81. [PubMed: 16476569]
10. Fuqua C, Greenberg EP. Listening in on bacteria: acyl-homoserine lactone signalling. Nat. Rev. Mol. Cell Biol. 2002; 3(9):685–695. [PubMed: 12209128]
11. Hughes DT, Sperandio V. Inter-kingdom signalling: communication between bacteria and their hosts. Nat. Rev. Microbiol. 2008; 6(2):111–120. [PubMed: 18197168]
12. Rumbaugh KP, Griswold JA, Hamood AN. The role of quorum sensing in the in vivo virulence of Pseudomonas aeruginosa. Microbes. Infect. 2000; 2(14):1721–1731. [PubMed: 11137045]
13. Chhabra SR, Harty C, Hooi DSW, Daykin M, Williams P, Telford G, Pritchard DI, Bycroft BW. Synthetic analogues of the bacterial signal (quorum sensing) molecule N-(3-oxododecanoyl)-L-homoserine lactone as immune modulators. J. Med. Chem. 2003; 46(1):97–104. [PubMed: 12502363]
14. Ritchie AJ, Yam AOW, Tanabe KM, Rice SA, Cooley MA. Modification of In Vivo and In Vitro T- and B-Cell-Mediated Immune Responses by the Pseudomonas aeruginosa Quorum-Sensing Molecule N-(3-Oxododecanoyl)-l-Homoserine Lactone. Infect. Immun. 2003; 71(8):4421–4431. [PubMed: 12874321]
15. Telford G, Wheeler D, Williams P, Tomkins PT, Appleby P, Sewell H, Stewart GSAB, Bycroft BW, Pritchard DI. The Pseudomonas aeruginosaQuorum-Sensing Signal MoleculeN-(3-Oxododecanoyl)-l-Homoserine Lactone Has Immunomodulatory Activity. Infect. Immun. 1998; 66(1):36–42. [PubMed: 9423836]
16. Zimmermann S, Wagner C, Muller W, Brenner-Weiss G, Hug F, Prior B, Obst U, Hansch GM. Induction of neutrophil chemotaxis by the quorum-sensing molecule N-(3-oxododecanoyl)-L-homoserine lactone. Infect. Immun. 2006; 74(10):5687–5692. [PubMed: 16988244]
17. Davis BM, Jensen R, Williams P, O'Shea P. The interaction of N-acylhomoserine lactone quorum sensing signaling molecules with biological membranes: implications for inter-kingdom signaling. PLoS One. 2010; 5(10) e13522.
18. Ritchie AJ, Whittall C, Lazenby JJ, Chhabra SR, Pritchard DI, Cooley MA. The immunomodulatory Pseudomonas aeruginosa signalling molecule N-(3-oxododecanoyl)-L-homoserine lactone enters mammalian cells in an unregulated fashion. Immunol. Cell. Biol. 2007; 85(8):596–602. [PubMed: 17607318]
19. Jakubczyk D, Barth C, Kubas A, Anastassacos F, Koelsch P, Fink K, Schepers U, Brenner-Weiß G, Bräse S. Deuterium labelled N-acyl-L-homoserine lactones (AHLs) – interkingdom signalling

molecules - synthesis, structural studies, and interactions with model lipid membranes. Anal. Bioanal. Chem. 2012; 403(2):473–482. [PubMed: 22367286]

20. Franken PA, Hill AE, Peters CW, Weinreich G. Generation of Optical Harmonics. Phys. Rev. Lett. 1961; 7(4):118–119.
21. Shen YR. Surface properties probed by second-harmonic and sum-frequency generation. Nature. 1989; 337(6207):519–525.
22. Chen XY, Boughton AP, Tesmer JJG, Chen Z. In situ investigation of Heterotrimeric G protein beta gamma subunit binding and orientation on membrane bilayers. J. Am. Chem. Soc. 2007; 129(42) 12658-+
23. Chen XY, Chen Z. SFG studies on interactions between antimicrobial peptides and supported lipid bilayers. Biochim. Biophys. Acta, Biomembr. 2006; 1758(9):1257–1273.
24. Chen XY, Wang J, Kristalyn CB, Chen Z. Real-time structural investigation of a lipid bilayer during its interaction with melittin using sum frequency generation vibrational spectroscopy. Biophys. J. 2007; 93(3):866–875. [PubMed: 17483186]
25. Liu J, Conboy JC. Phase transition of a single lipid bilayer measured by sum-frequency vibrational spectroscopy. J. Am. Chem. Soc. 2004; 126(29):8894–8895. [PubMed: 15264810]
26. Liu J, Conboy JC. Direct measurement of the transbilayer movement of phospholipids by sum-frequency vibrational spectroscopy. J. Am. Chem. Soc. 2004; 126(27):8376–8377. [PubMed: 15237984]
27. Kett PJN, Casford MTL, Davies PB. Sum Frequency Generation (SFG) Vibrational Spectroscopy of Planar Phosphatidylethanolamine Hybrid Bilayer Membranes under Water. Langmuir. 2010; 26(12):9710–9719. [PubMed: 20394443]
28. Pohle W, Saβ M, Selle C, Wolfrum K, Löbau J. Probing phospholipid chain fluidity by vibrational spectroscopy including sum-frequency generation. Vib. Spectrosc. 1999; 19(2):321–327.
29. Tong Y, Li N, Liu H, Ge A, Osawa M, Ye S. Mechanistic Studies by Sum-Frequency Generation Spectroscopy: Hydrolysis of a Supported Phospholipid Bilayer by Phospholipase A2. Angew. Chem. Int. Ed. 2010; 49(13):2319–2323.
30. Avery CW, Som A, Xu Y, Tew GN, Chen Z. Dependence of Antimicrobial Selectivity and Potency on Oligomer Structure Investigated Using Substrate Supported Lipid Bilayers and Sum Frequency Generation Vibrational Spectroscopy. Anal. Chem. 2009; 81(20):8365–8372. [PubMed: 19754103]
31. Avery CW, Palermo EF, McLaughlin A, Kuroda K, Chen Z. Investigations of the Interactions between Synthetic Antimicrobial Polymers and Substrate-Supported Lipid Bilayers Using Sum Frequency Generation Vibrational Spectroscopy. Anal. Chem. 2011; 83(4):1342–1349. [PubMed: 21229969]
32. Thennarasu S, Huang R, Lee D-K, Yang P, Maloy L, Chen Z, Ramamoorthy A. Limiting an Antimicrobial Peptide to the Lipid-Water Interface Enhances Its Bacterial Membrane Selectivity: A Case Study of MSI-367. Biochemistry. 2010; 49(50):10595–10605. [PubMed: 21062093]
33. Chen X, Tang H, Even MA, Wang J, Tew GN, Chen Z. Observing a Molecular Knife at Work. J. Am. Chem. Soc. 2006; 128(8):2711–2714. [PubMed: 16492058]
34. Chen X, Wang J, Boughton AP, Kristalyn CB, Chen Z. Multiple Orientation of Melittin inside a Single Lipid Bilayer Determined by Combined Vibrational Spectroscopic Studies. J. Am. Chem. Soc. 2007; 129(5):1420–1427. [PubMed: 17263427]
35. Nguyen KT, Soong R, lm S-C, Waskell L, Ramamoorthy A, Chen Z. Probing the Spontaneous Membrane Insertion of a Tail-Anchored Membrane Protein by Sum Frequency Generation Spectroscopy. J. Am. Chem. Soc. 2010; 132(43):15112–15115. [PubMed: 20932011]
36. Nguyen TT, Rembert K, Conboy JC. Label-Free Detection of Drug-Membrane Association Using Ultraviolet-Visible Sum-Frequency Generation. J. Am. Chem. Soc. 2009; 131(4):1401–1403. [PubMed: 19140762]
37. Nguyen KT, Le Clair SpV, Ye S, Chen Z. Molecular Interactions between Magainin 2 and Model Membranes in Situ. J. Phys. Chem. B. 2009; 113(36):12358–12363. [PubMed: 19728722]
38. Nguyen KT, King JT, Chen Z. Orientation Determination of Interfacial β-Sheet Structures in Situ. J. Phys. Chem. B. 2010; 114(25):8291–8300. [PubMed: 20504035]

39. Wang T, Li D, Lu X, Khmaladze A, Han X, Ye S, Yang P, Xue G, He N, Chen Z. Single Lipid Bilayers Constructed on Polymer Cushion Studied by Sum Frequency Generation Vibrational Spectroscopy. J. Phys. Chem. C. 2011; 115(15):7613–7620.
40. Ye S, Nguyen KT, Chen Z. Interactions of Alamethicin with Model Cell Membranes Investigated Using Sum Frequency Generation Vibrational Spectroscopy in Real Time in Situ. J. Phys. Chem. B. 2010; 114(9):3334–3340. [PubMed: 20163089]
41. Kim J, Kim G, Cremer PS. Investigations of Water Structure at the Solid/Liquid Interface in the Presence of Supported Lipid Bilayers by Vibrational Sum Frequency Spectroscopy. Langmuir. 2001; 17(23):7255–7260.
42. Yang P, Ramamoorthy A, Chen Z. Membrane Orientation of MSI-78 Measured by Sum Frequency Generation Vibrational Spectroscopy. Langmuir. 2011; 27(12):7760–7767. [PubMed: 21595453]
43. Ye S, Nguyen KT, Clair SVL, Chen Z. In situ molecular level studies on membrane related peptides and proteins in real time using sum frequency generation vibrational spectroscopy. J. Struct. Biol. 2009; 168(1):61–77. [PubMed: 19306928]
44. Kriech MA, Conboy JC. Using the Intrinsic Chirality of a Molecule as a Label-Free Probe to Detect Molecular Adsorption to a Surface by Second Harmonic Generation. Appl. Spectrosc. 2005; 59(6):746–753. [PubMed: 16053540]
45. Conboy JC, Kriech MA. Measuring melittin binding to planar supported lipid bilayer by chiral second harmonic generation. Anal. Chim. Acta. 2003; 496(1–2):143–153.
46. Andersson AS, Glasmastar K, Sutherland D, Lidberg U, Kasemo B. Cell adhesion on supported lipid bilayers. J. Biomed. Mater. Res., Part A. 2003; 64A(4):622–629.
47. Briand E, Zach M, Svedhem S, Kasemo B, Petronis S. Combined QCM-D and EIS study of supported lipid bilayer formation and interaction with pore-forming peptides. Analyst. 2010; 135(2):343–350. [PubMed: 20098769]
48. Richter RP, Berat R, Brisson AR. Formation of solid-supported lipid bilayers: An integrated view. Langmuir. 2006; 22(8):3497–3505. [PubMed: 16584220]
49. Diesner M-O, Welle A, Kazanci M, Kaiser P, Spatz J, Koelsch P. In vitro observation of dynamic ordering processes in the extracellular matrix of living, adherent cells. Biointerphases. 2011; 6(4): 171–179. [PubMed: 22239810]
50. Verreault D, Kurz V, Howell C, Koelsch P. Sample cells for probing solid/liquid interfaces with broadband sum-frequency-generation spectroscopy. Rev. Sci. Instrum. 2010; 81(6)
51. Kurz V, Grunze M, Koelsch P. In Situ Characterization of Thermo-Responsive Poly(N-Isopropylacrylamide) Films with Sum-Frequency Generation Spectroscopy. ChemPhysChem. 2010; 11(7):1425–1429. [PubMed: 20217885]
52. Howell C, Maul R, Wenzel W, Koelsch P. Interactions of hydrophobic and hydrophilic self-assembled monolayers with water as probed by sum-frequency-generation spectroscopy. Chem. Phys. Lett. 2010; 494(4–6):193–197.
53. Diesner MO, Howell C, Kurz V, Verreault D, Koelsch P. In Vitro Characterization of Surface Properties Through Living Cells. J. Phys. Chem. Lett. 2010; 1(15):2339–2342.
54. Howell C, Schmidt R, Kurz V, Koelsch P. Sum-frequency-generation spectroscopy of DNA films in air and aqueous environments. Biointerphases. 2008; 3(3):Fc47–Fc51. [PubMed: 20408693]
55. Howell C, Diesner MO, Grunze M, Koelsch P. Probing the Extracellular Matrix with Sum-Frequency-Generation Spectroscopy. Langmuir. 2008; 24(24):13819–13821. [PubMed: 19053661]
56. Lagutchev A, Hambir SA, Dlott DD. Nonresonant background suppression in broadband vibrational sum-frequency generation spectroscopy. J. Phys. Chem. C. 2007; 111(37):13645–13647.
57. Curtis AD, Asplund MC, Patterson JE. Use of Variable Time-Delay Sum-Frequency Generation for Improved Spectroscopic Analysis. J. Phys. Chem. C. 2011; 115(39):19303–19310.
58. Curtis AD, Burt SR, Calchera AR, Patterson JE. Limitations in the Analysis of Vibrational Sum-Frequency Spectra Arising from the Nonresonant Contribution. J. Phys. Chem. C. 2011; 115(23): 11550–11559.
59. Quast AD, Curtis AD, Horn BA, Goates SR, Patterson JE. Role of Nonresonant Sum-Frequency Generation in the Investigation of Model Liquid Chromatography Systems. Anal. Chem. 2012; 84(4):1862–1870. [PubMed: 22264066]

60. Yang CSC, Richter LJ, Stephenson JC, Briggman KA. In Situ, Vibrationally Resonant Sum Frequency Spectroscopy Study of the Self-Assembly of Dioctadecyl Disulfide on Gold. Langmuir. 2002; 18(20):7549–7556.

61. Ward RN, Davies PB, Bain CD. Orientation of Surfactants Adsorbed on a Hydrophobic Surface. J. Phys. Chem. 1993; 97(28):7141–7143.

62. Schachtschneider JH, Snyder RG. Vibrational analysis of the n-paraffins-II: Normal co-ordinate calculations. Spectrochim. Acta. 1963; 19(1):117–168.

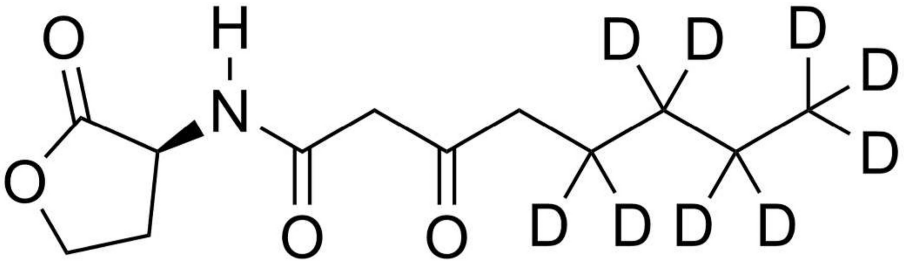

1a

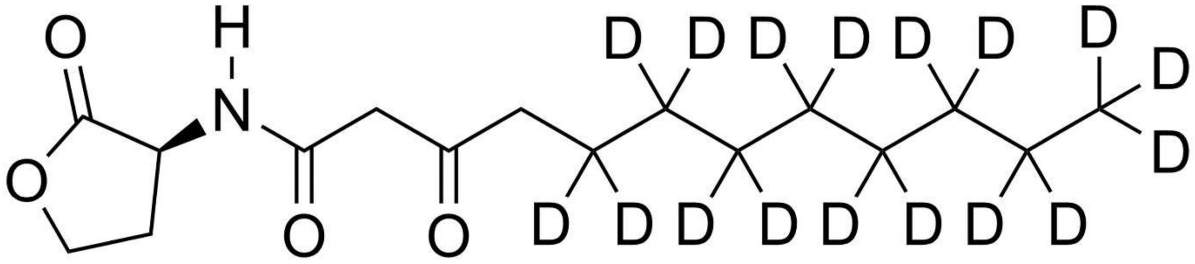

1b

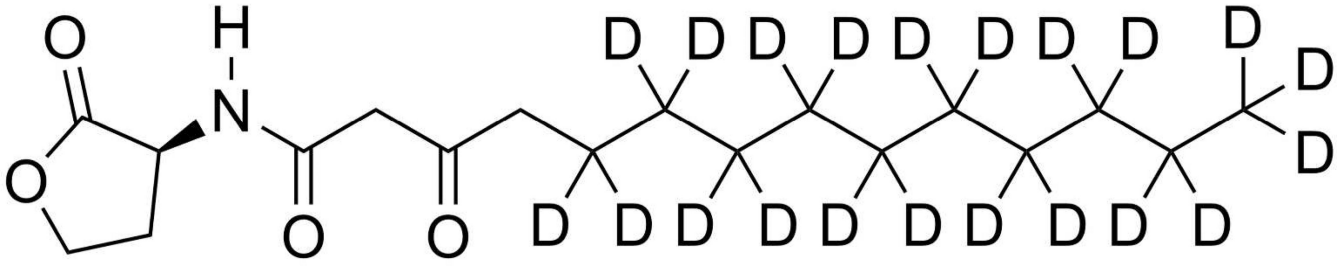

1c

Figure 1.

The structure of the deuterated AHLs (AHL-d_n): *N*-(3-oxooctanoyl-d_9)-L-homoserine lactone (AHL-d_9; 1a), *N*-(3-oxododecanoyl-d_{17})-L-homoserine lactone (AHL-d_{17}; 1b), and *N*-(3-oxotetradecanoyl-d_{21})-L-homoserine lactone (AHL-d_{21}; 1c)

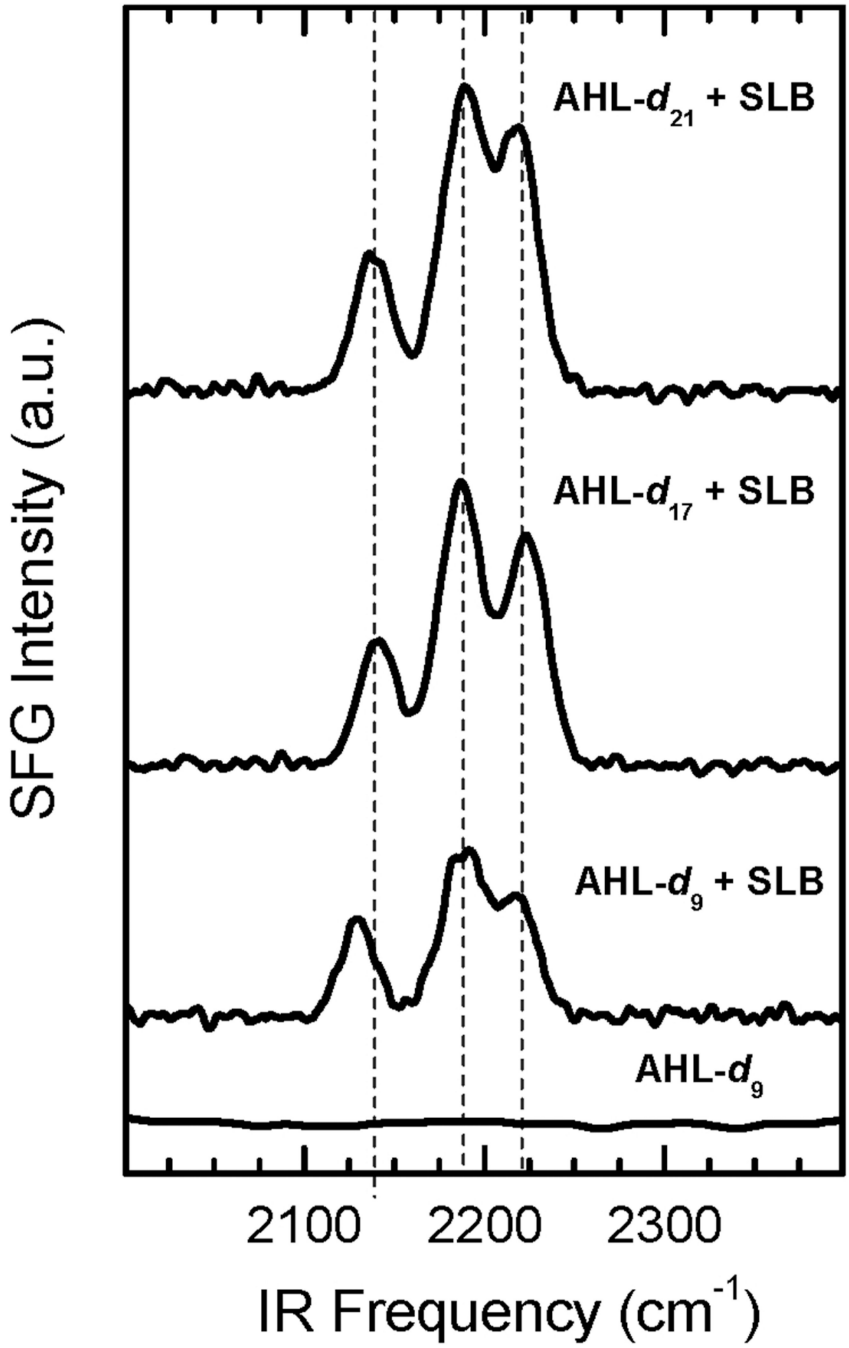

Figure 2.

Background-suppressed SFG spectra in the spectral region of deuterated methyl and methylene groups for AHL-d_9 in solution and for the three AHL derivatives AHL-d_9, AHL-d_{17}, and AHL-d_{21} in the presence of the SLB. Only in the presence of AHL-d_n and the SLB can an SFG signal be detected. This increases in intensity with increasing chain length. Prominent peak positions are marked as dotted vertical lines.

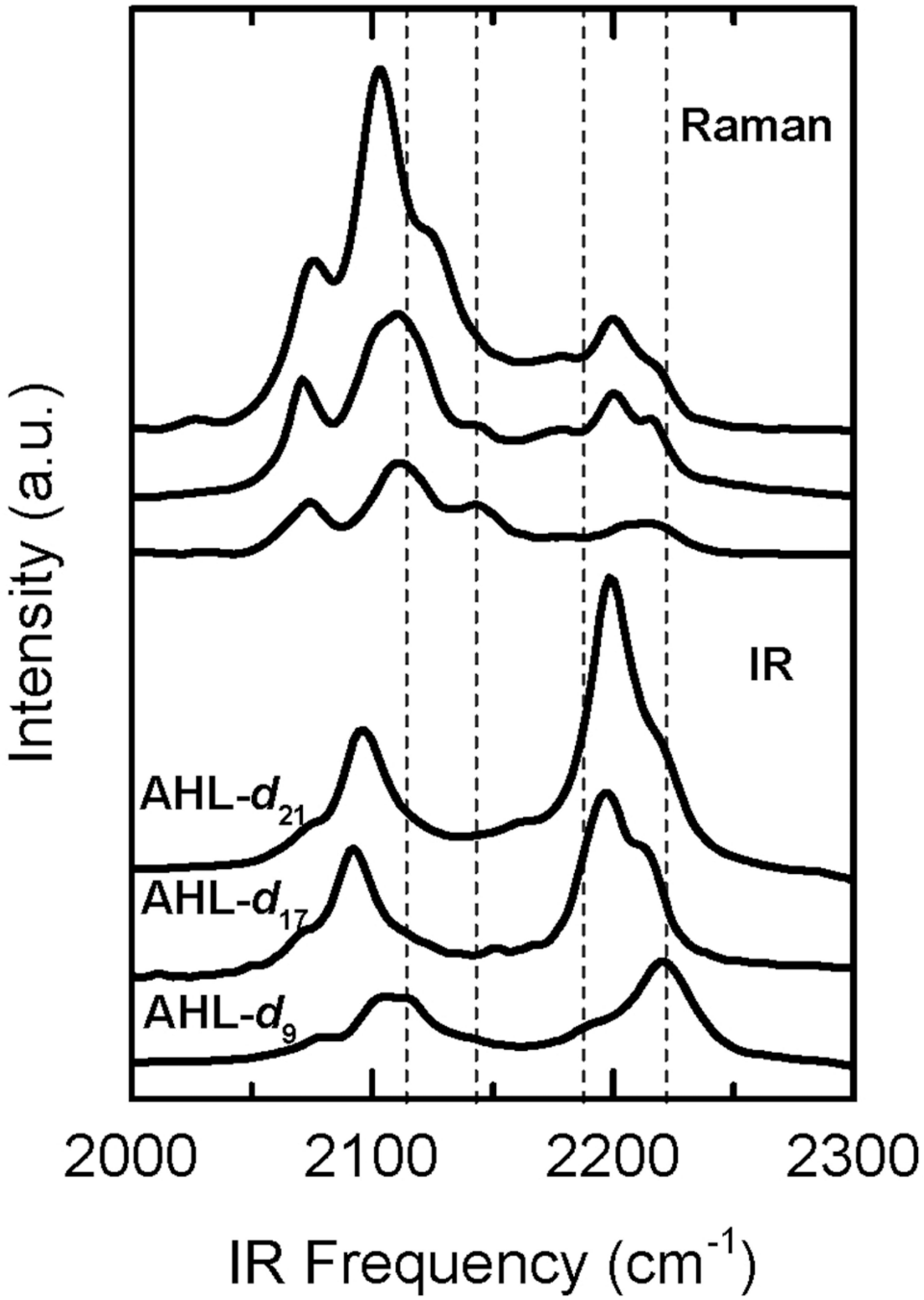

Figure 3.
IR (bottom 3) and Raman (top 3) spectra of incorporated AHL-d_n derivatives in its solid state. The bands that get more prominent with decreasing chain length can be associated to CD_3 vibrations (dotted vertical lines) and coincide in peak positions to the ones detected in the SFG spectra of incorporated AHL-d_n (Fig. 2).

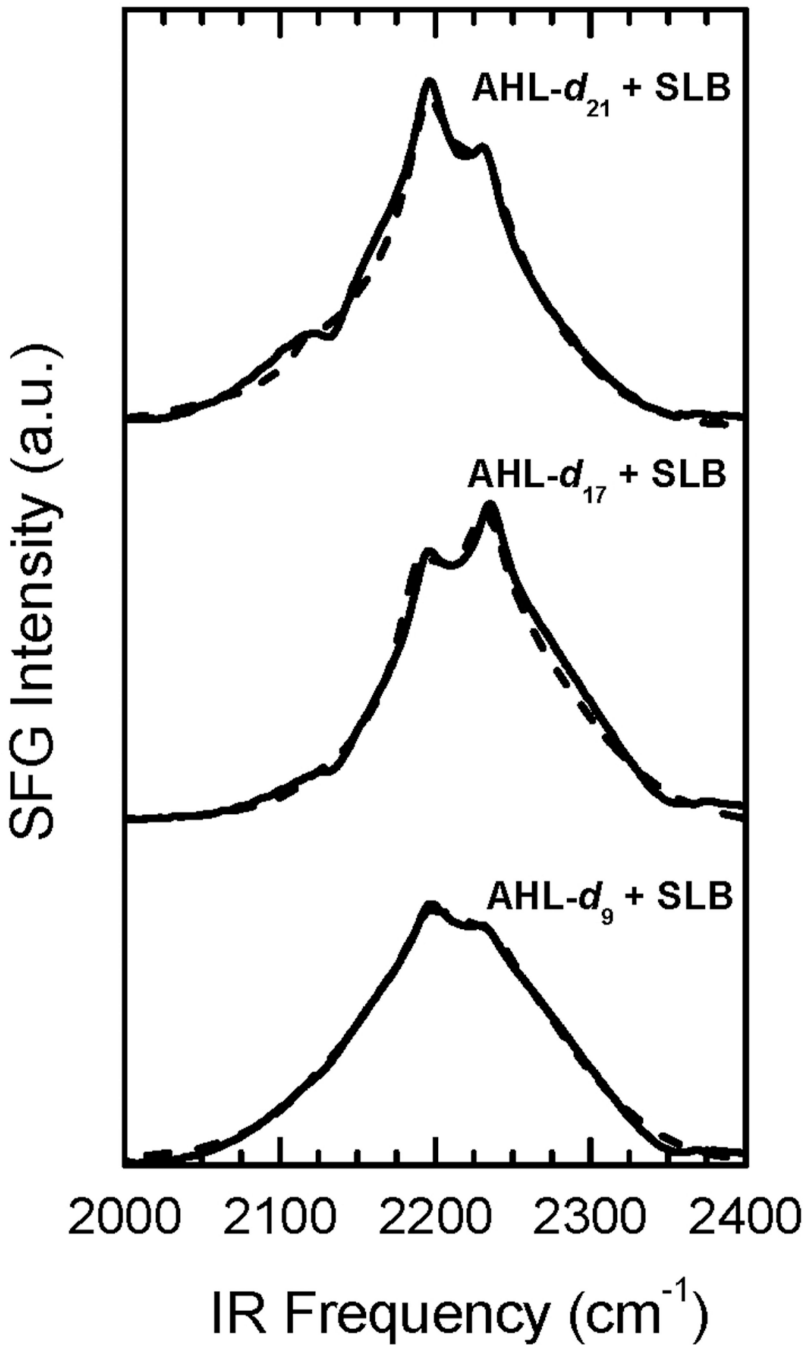

Figure 4.

Non background-suppressed SFG spectra of incorporated AHL-d_9, AHL-d_{17}, and AHL-d_{21}. The envelope reflects the non-resonant signal of the Au layer with a Gaussian-like IR intensity profile. The r^- band located at 2220 cm^{-1} has a constructive relative phase to the non-resonant background resulting in a peak in the spectrum. The appearance of a peak in the spectrum is an indicator for a deuterated methyl group pointing towards the surface. Fits of the spectra are plotted as dotted lines.

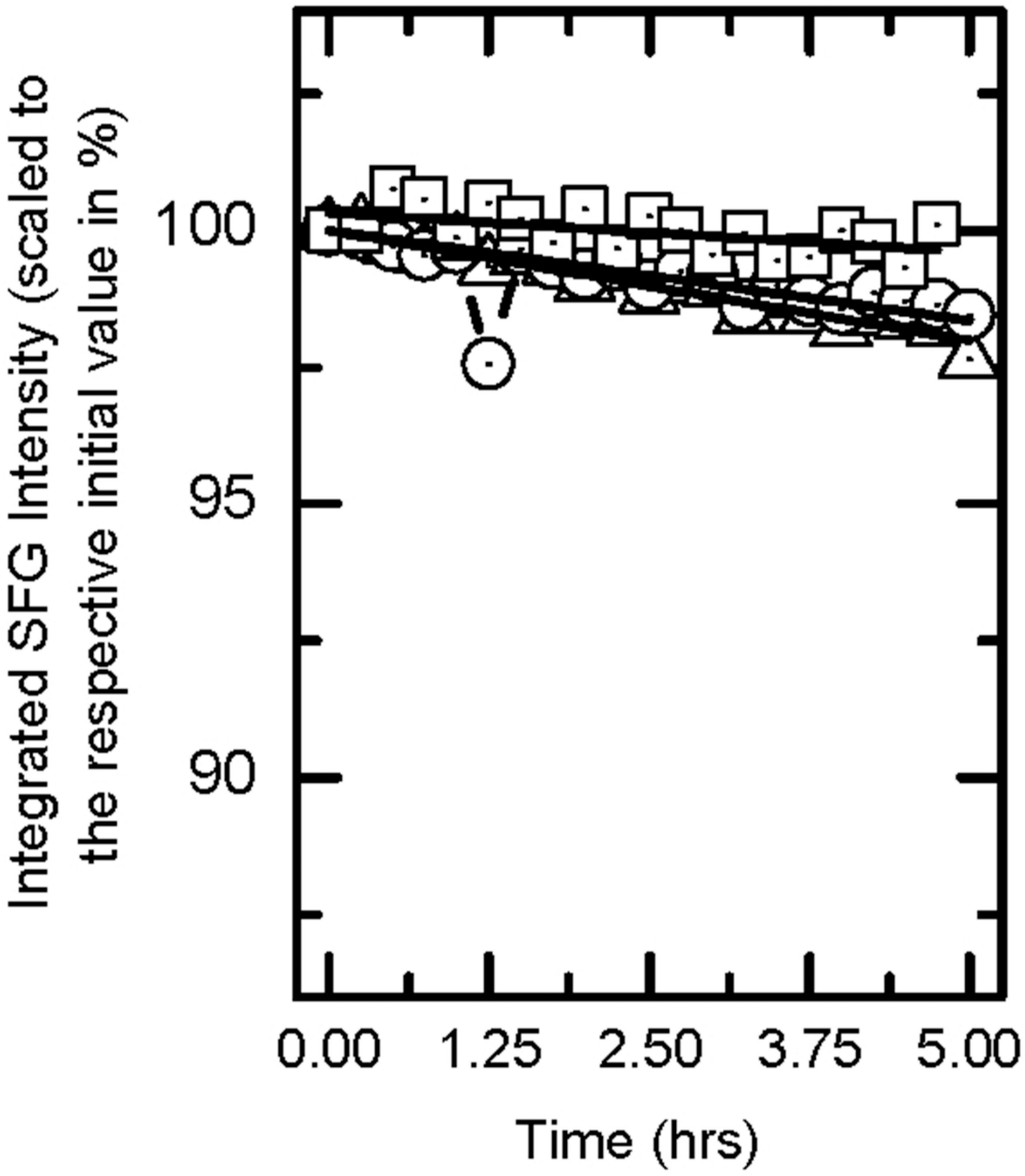

Figure 5.
Integrated SFG intensities of the background-suppressed spectra for AHL-d_{21} (triangles), AHL-d_{17} (circles) and AHL-d_9 (squares). Values are normalized to their respective initial intensities. Full lines are exponential fits as described in the text.

Table 1

Fitting results for the CD_3 asym. vibrational stretching mode of incorporated AHL-d_n.

AHL-d_n + SLB	**ω_r-(cm^{-1})**	**ϕ_k (°)**
AHL-d_9 + SLB	2218	−63 ± 15
AHL-d_{17} + SLB	2223	−9 ± 15
AHL-d_{21} + SLB	2219	−31 ± 15

Table 2

Determined decay constants and half-lives of incorporated AHL-d_n.

AHL-d_n + SLB	**Decay constant k (10^{-4} s^{-1})**	**Half-lives $T_{1/2}$ (days)**
AHL-d_{21} + SLB	2.55 ± 0.08	14.2 ± 0.4
AHL-d_{17} + SLB	2.07 ± 0.02	17.4 ± 0.2
AHL-d_9 + SLB	0.9 ± 0.3	112 ± 40